KERNFORSCHUNGSZENTRUM

KARLSRUHE

Mai 1965

KFK 303
SM 62/3

Institut für Neutronenphysik und Reaktortechnik

Pulsed Source and Noise Measurements on the STARK-Reactor at Karlsruhe

M. Edelmann, G. Kussmaul, H. Meister, D. Stegemann, W. Väth

GESELLSCHAFT FÜR KERNFORSCHUNG M. B. H.

KARLSRUHE

KERNFORSCHUNGSZENTRUM KARLSRUHE

May 1965

KFK 303

SM 62/3

Institut für Neutronenphysik und Reaktortechnik

Pulsed Source and Noise Measurements on the STARK-Reactor at Karlsruhe

M.Edelmann, G.Kussmaul, H.Meister, D.Stegemann, W.Väth

Gesellschaft für Kernforschung m.b.H. Karlsruhe

INTERNATIONAL ATOMIC ENERGY AGENCY

SYMPOSIUM ON PULSED NEUTRON RESEARCH

May 10 - 14, 1965
Kernforschungszentrum Karlsruhe, Germany

SM 62/3

PULSED SOURCE AND NOISE MEASUREMENTS ON THE STARK-REACTOR AT KARLSRUHE +

M.Edelmann, G.Kußmaul, H.Meister, D.Stegemann, W.Väth
Kernforschungszentrum Karlsruhe

1. Introduction

For the determination of kinetic reactor physics parameters, such as the prompt neutron decay constant α, the neutron generation time and related quantities, different experimental methods can be applied. The pulsed neutron source technique and the analysis of statistical phenomena due to branching processes in neutron chains within the reactor are the most powerful tools for these investigations. It was therefore decided early to look into both possibilities in order to have the best approach for the determination of reactor parameters, particularly in the Fast Zero Power Assembly SNEAK and the Fast Thermal Argonaut Reactor STARK. The main purpose of the experiments reported in this paper was to obtain a comparison of results which were measured under exactly the same loading and reactivity conditions in STARK first by the pulsed neutron source technique and then by three different statistical methods, i.e., the Rossi-α-experiment, the analysis of counting statistics, and the frequency analysis of noise. Although the results are specific for this particular reactor system, the comparison should give some insight into the general problems and limitations of the different techniques.

+ The work was performed within the frame of the Fast Breeder Project-Association Karlsruhe-Euratom

2. Description of the system

The STARK-reactor was designed as a coupled fast-thermal zero-power reactor. A detailed description of the assembly and a discussion of its safety features have been given previously [1].

Basically, the reactor consists of a cylindrical fast core (37 cm average diameter, 61 cm height) which is surrounded by an annular Argonaut-type thermal driver zone and a large graphite reflector. As shown in fig.1, the fast core is an array of 37 vertical stainless steel matrix tubes filled with the core materials to be investigated. The fast core is enclosed in a natural uranium buffer zone of 5 cm average thickness to absorb thermal neutrons incident from the outside.

The present investigations were carried out on the first loading of STARK in which the central zone was filled with natural uranium metal. The thermal zone contained 364 Argonaut fuel plates (U^{235}-content = 7.58 kg) arranged in 24 groups with a plate spacing of 6.2 mm. The moderator was light water at 79°C.

According to fission chamber traverses, only about 1% of the reactor power is produced by fast fissions in the natural uranium zone so that the reactor can be considered essentially as a thermal system. Actually, the central zone causes a strong decoupling of opposite portions of the annular thermal core.

The control system of the reactor consists of 12 cadmium-plate control units of equal size, evenly distributed around the thermal core. Three of them (R_1, R_2, and R_3) are normally used as fine control plates, the others as safety plates (fig.1). For these experiments, however, the plate S_3^3 was used to adjust criticality with all other plates fully withdrawn. Hence, various subcritical states (fig.1) were obtained by inserting groups of control plates while S_3^3 was kept in its original position.

The location of the neutron detectors (BF_3-counters, boron chambers, and a U^{235}-fission chamber) used for the various experiments is also shown in fig.1. Since the flux distribution in the annular core was known to be very sensitive to small loading changes, the detectors were always kept in their positions and no changes were made from one experiment to the other.

Fig.1

Schematic cross section of STARK with detector positions

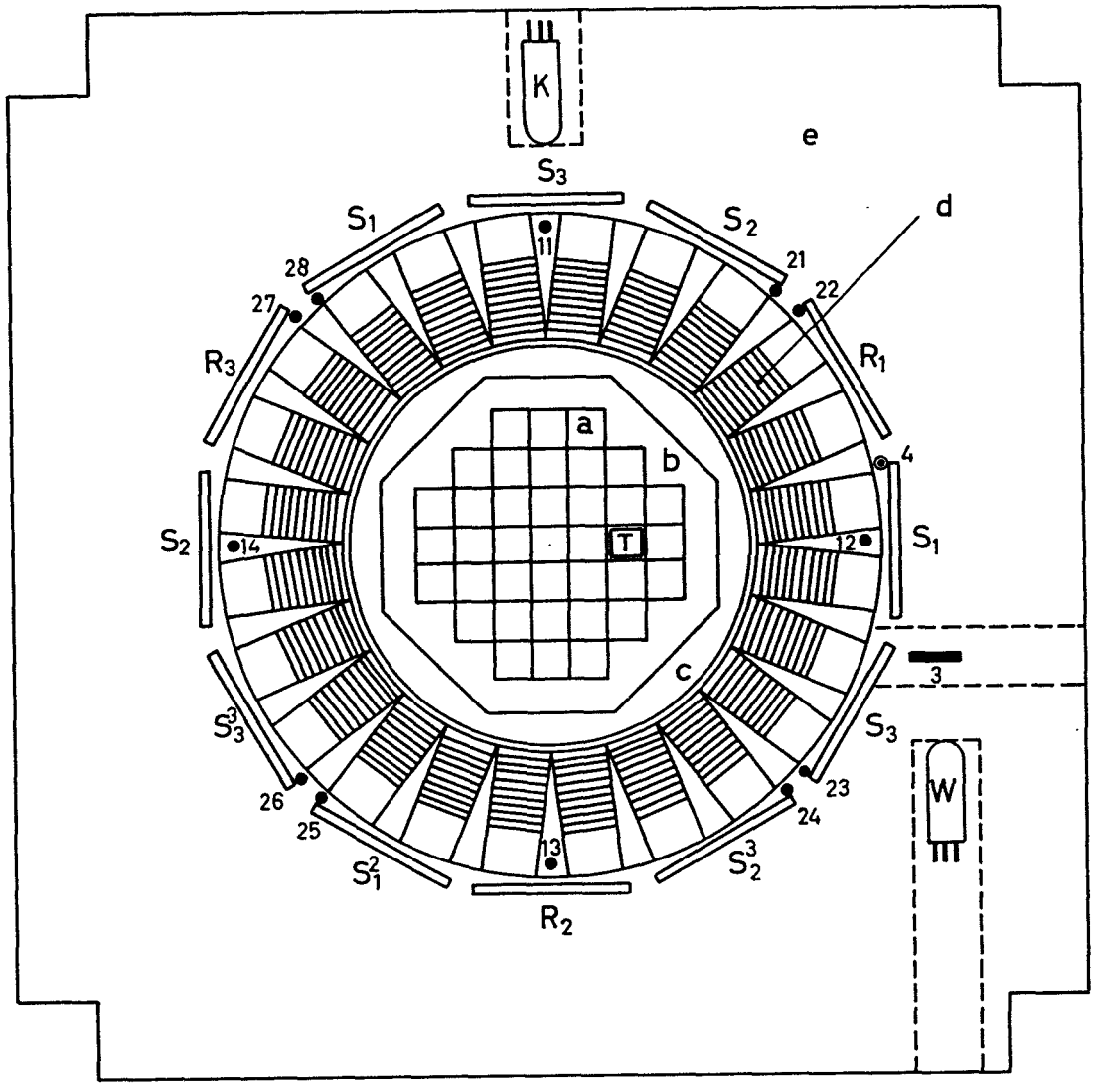

a - fast core, b - natural uranium casing, c - graphite region
d - thermal Argonaut core, e - graphite reflector
R - fine control plates, S - safety plates, T - safety rod of fast core
● and ▬ BF_3-proportional counters, ◎ U^{235}-fission chamber
⊂≡ B^{10}-γ-compensated ionisation chamber

Description of reactor configurations investigated

Conf. No.	Position of control and safety plates	Conf. No.	Position of control and safety plates
I	delayed critical [1]	VI	R_3 in [1]
II	R_2 on 35 cm [1]	VII	S_1^2, R_2, and S_2^3 in [1]
III	R_2 on 20 cm [1]	VIII	R_1, R_2, and R_3 in [1]
IV	R_2 in [1]	IX	all S_1 and S_2 in [1]
V	R_1 in [1]	X	all plates in

Plate positions go from 0 (in) to 47 cm (out).
[1] All other plates out except S_3^3 which is in critical pos. 30.7 cm.

3. Pulsed source experiments

3.1 Methods

Three different evaluation techniques have been described in the literature to determine reactivity ρ and prompt-neutron generation time Λ of a multiplying system from a pulsed source experiment. All of them are based on the observation of the neutron density n(t) as a function of time resulting from the injection of a periodic sequence of neutron bursts. As is well known, n(t) is composed of an exponential decay of the prompt eigenfunction, $n_p(t)$, followed by a slowly varying delayed neutron part $n_d(t)$ which is usually assumed to be time-independent, $n_d(t) \approx n_d(o)$ within a cycle ($o < t < T$). Thus, for the fundamental mode one has

$$n(t) = n_p(t) + n_d(t) = A\, e^{-\alpha t} + n_d(t) \,. \tag{3.1}$$

(1) The first method [2] makes use of the prompt part only, $n_p(t)$, from which the prompt-neutron decay constant

$$\alpha = \frac{\beta}{\Lambda} \left(1 - \frac{\rho}{\beta}\right) \tag{3.2}$$

is derived. Hence, the reactivity ρ/β can be determined, either using calculated values of Λ and β, or the decay constant $\alpha_c = \beta/\Lambda_c$ measured at delayed critical and assuming Λ to be independent of ρ :

$$-\rho/\beta = \alpha/\alpha_c - 1 \tag{3.3}$$

(2) Sjöstrand [3] and Gozani [4] have shown that for an unreflected system

$$-\rho/\beta = \bar{n}_p/\bar{n}_d \tag{3.4}$$

where $\bar{n}_p$, $\bar{n}_d$ are the time-averaged quantities $n_p(t)$ and $n_d(t)$. Combining eqs.(3.2) and (3.4) one finds

$$\beta/\Lambda = \frac{\alpha}{1 + \bar{n}_p/\bar{n}_d} \tag{3.5}$$

from which the generation time Λ can be derived.

(3) The third method developed by Garelis and Russell [5 - 7] allows one to determine $\gamma = \beta/\Lambda$ from $n_p(t)$ and $n_d(t)$ using the equation

$$\int_o^T n_p(t) \left[e^{\gamma t} - 1 \right] dt = \int_o^T n_d(t)\, dt \tag{3.6}$$

(T = cycle length) which has been derived from a one-group model for an unreflected system. Eq.(3.6) is also valid for mixtures of eigenfunctions if Λ is independent of ρ.

Method (3) was originally derived for a constant delayed-neutron density, $n_d(t) = \text{const}$. For measurements on thermal systems close to delayed critical, however, the variation of $n_d(t)$, which is caused by the build-up of precursors during the decay of $n_p(t)$, becomes important and the question arises how to split n(t) into prompt and delayed parts. We define $n_p(t)$ and $n_d(t)$ in accordance with the usual space-independent kinetic equations [8] by

$$\begin{aligned} \frac{\rho-\beta}{\Lambda}\, n_p + q\,\delta(t) &= \frac{dn_p}{dt} \\ \frac{\rho-\beta}{\Lambda}\, n_d + \sum_{i=1}^{6} \lambda_i C_i &= \frac{dn_d}{dt} \\ \frac{\beta_i}{\Lambda}\,(n_p + n_d) - \lambda_i C_i &= \frac{dC_i}{dt} \qquad (i = 1, \ldots 6)\ . \end{aligned} \tag{3.7}$$

Eq.(3.4) is valid only with this definition of n_p and n_d. This can be shown by integrating eq.(3.7) over a cycle ($o < t < T$). Also eq.(3.6) holds as a consequence of eqs.(3.2) and (3.4).

For the evaluation of the experimental decay curves, with $\rho < 0$, an approximate expression for $n_d(t)$ has been derived by an iteration process. Starting with $n(t) = n_p(o)\, e^{-\alpha t} + b$ as a first guess and using

$$C_i(t) = \frac{\beta_i}{\Lambda} \int_{-\infty}^{t} n(t')\, e^{-\lambda_i (t-t')}\, dt'\ ,$$

and

$$n_d(t) = \sum_{i=1}^{6} \lambda_i \int_{-\infty}^{t} C_i(t')\, e^{-\alpha(t-t')}\, dt' \tag{3.8}$$

which follows from eq.(3.7), we finally arrive at

$$n_d(t) = n_d(o) + n_p(o)\, \frac{\alpha_c \bar{\lambda}}{\alpha^2} \left[\left(1 - \frac{t}{T}\right) - (1 + \alpha t)\, e^{-\alpha t} \right] \tag{3.9}$$

and

$$\bar{n}_d = n_d(o) \left[1 - \frac{1}{2}\, \frac{\rho}{\beta - \rho}\, \bar{\lambda} \cdot T \right], \qquad \bar{\lambda} = \sum_{i=1}^{6} \beta_i \lambda_i / \beta\ . \tag{3.10}$$

These are valid for $\lambda_i \ll \alpha$ and $\lambda_i T \ll 1$. These equations allow the calculation of $n_d(t)$ and $\bar{n}_d$ from the value $n_d(T) = n_d(o)$, which is measured by the background channel of the time analyser.

3.2 Experiments

A number of systems with different control plate configurations (fig.1), ranging in reactivity from delayed critical down to -8 $ subcritical, have been investigated by the pulsed source technique using the three different evaluation techniques outlined in section 3.1.

A compact 100 kev deuteron accelerator with duoplasmatron ion-source [9] was used as a pulsed neutron generator. The unit was fed through the central hole of the top shield of the reactor so that the tritium target was located on top of the natural uranium zone. BF_3-counters as neutron detectors were placed in three different radial positions (fig.1): in the graphite wedge between the fuel plates of the thermal core (Pos.12), in the graphite reflector (Pos.3), and in the air gap between core and reflector (Pos.24).

The decay of the neutron intensity n(t) following each neutron burst (pulse width 10 or 20 μsec) was measured with a 256-channel analyser (TMC, Model CN-110) with pulsed neutron input unit. The pulsed source was synchronized with the analyser in such a way that the first channel opened at the time when the neutron burst was injected. The repetition rate f = 1/T of the source was chosen low enough that the contribution of prompt neutrons to the background data, which were taken at the very end of each cycle, was negligibly small.

All measurements on subcritical systems were done under stationary-state conditions. In order to saturate the delayed neutron density $n_d(t)$, the pulsed source was kept in operation at constant intensity for 5 to 10 min before actual data were taken. The background data contained, in addition to the delayed neutrons, the effect of the spontaneous fission sources in the natural uranium. This effect was determined in a separate run without pulsed source and subtracted.

For an evaluation of the prompt-neutron decay $n_p(t)$, the slowly varying delayed part $n_d(t)$ was subtracted from the data. As a first approximation $n_d(t)$ was assumed to be a time-independent background given by the neutron intensity at the end of the cycle, $n_d(t) = n(T)$. This treatment was adequate for all subcritical measurements below -0.5 $. For the measurements closer to delayed critical the delayed neutron build-up during the decay of the prompt part given by eq.(3.9) was taken into account:

$$n_p(t) = \frac{n(t) - n_d(o)}{1 + F(\alpha, t)} \quad , \quad F(\alpha,T) = \frac{\alpha_c \bar{\lambda}}{\alpha^2} \left[(1 - \frac{t}{T}) e^{\alpha t} - (1+\alpha t) \right] \qquad (3.11)$$

Fig.2 shows the effect of this second-order correction on the prompt-neutron decay curve at delayed critical. The decay constant was obtained by fitting an exponential function $e^{-\alpha t}$ to the later part of the curve $n_p(t)$, where contributions of higher modes are negligible. The α-values found in the three detector positions are listed in table I.

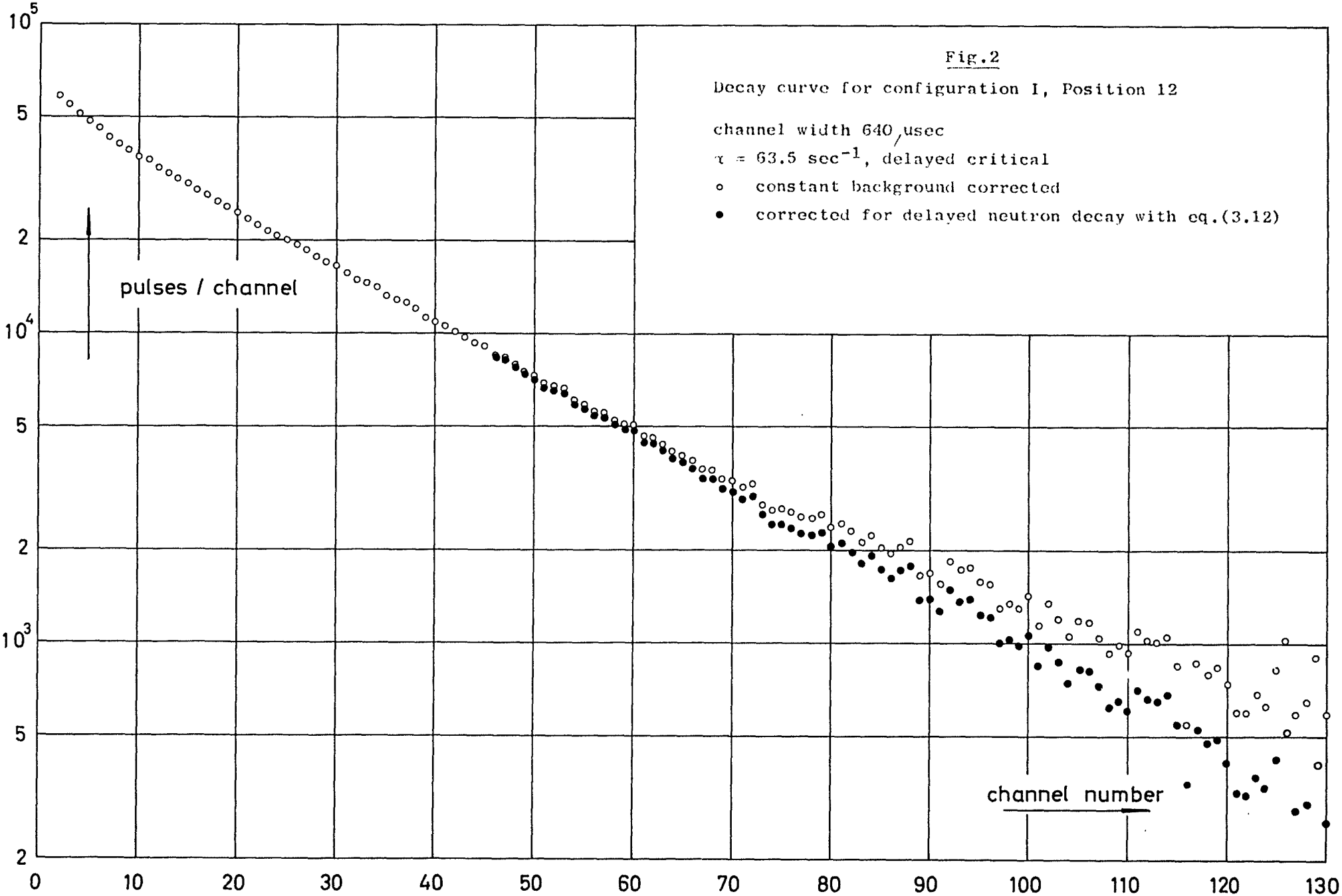

Fig.2

Decay curve for configuration I, Position 12

channel width 640 μsec

$\alpha = 63.5\ \text{sec}^{-1}$, delayed critical

○ constant background corrected

● corrected for delayed neutron decay with eq.(3.12)

The ratio of the average prompt and delayed neutron intensities, $\bar{n}_p/\bar{n}_d$, was also derived from the decay curves. The quantity $\bar{n}_p$ was found by extrapolating the fundamental mode decay back to t = o, assuming zero slowing-down time. From the extrapolated value $n_o = n_p(t = o)$ one finds $\bar{n}_p = n_o/\alpha$. The delayed neutron part $\bar{n}_d$ was obtained from the neutron intensity at the end of the cycle, $n(T) = n_d(T)$, using eq.(3.10). Contributions of higher modes to $\bar{n}_d$, which are expected to be small near delayed critical, cannot be eliminated with this technique.

Finally, the quantity $\gamma = \beta/\Lambda$ was determined by the method of Garelis and Russell, eq.(3.6). A Fortran code was written to evaluate the integral of the left hand side in eq.(3.6) as a function of γ from the experimental data $n_p(t)$ and $n_d(t)$, and the quantity $\gamma = \beta/\Lambda$ was sought for which eq.(3.6) is fulfilled.

For measurements of the prompt-neutron decay at delayed critical, the following procedure was adopted to keep the delayed neutron background at a reasonably low level ($\approx 0.3 \cdot n_p(o)$): Starting from a reactor power of ≈ 1 mWatt a sequence of only 150 source pulses was injected (f = 2 to 5 sec^{-1}) during which the delayed neutron intensity rose in a stepwise manner. Afterwards, the reactor power was brought down again to 1 mWatt by inserting a control plate, and the procedure was repeated several times to get a good statistical accuracy.

Corrections for the delayed neutron build-up were made on the basis of eq.(3.11) but using a somewhat different correction factor for the non-stationary case (cf.fig.2):

$$F(\alpha, T) = \frac{\bar{\lambda}}{\alpha_c} \left[(1 + b \cdot t)\, e^{\alpha t} - (1 + \alpha t) \right] . \qquad (3.12)$$

For most cases the constant b, which is a function of cycle length T, number of bursts injected, and the strength of internal sources, was found by a fit to the background data to be zero within experimental error.

3.3 Results

Tab.I gives the experimental results for the decay constant α and the ratio $\bar{n}_p/\bar{n}_d$. The quantity $\gamma = \beta/\Lambda$ as obtained from eq.(3.6) by the method of Garelis and Russell for the various control plate configurations is given in table II.

Tab. I Experimental results for decay constant α, reactivity $(\rho/\beta)_s$, and the ratio $\bar{n}_p/\bar{n}_d$

	α	α	α	$\alpha_{av.}$	$\alpha/\alpha_c - 1$	$-(\rho/\beta)_s$	$\bar{n}_p/\bar{n}_d$	$\bar{n}_p/\bar{n}_d$	$\bar{n}_p/\bar{n}_d$
Detector position (cf. fig.1)	(12)	(24)	(3)				(12)	(24)	(3)
Control plate configuration (cf.fig.1)	$[sec^{-1}]$	$[sec^{-1}]$	$[sec^{-1}]$	$[sec^{-1}]$	[$]	[$]	[$]	[$]	[$]
Delayed critical I	63.5		62.3	62.9±1.5					
R_2 : 35.0 cm II	69.0		69.5	69.2±1.5	0.100	0.085	0.093		0.100
R_2 : 20.0 cm III	85.4		85.2	85.3±1.5	0.356	0.332	0.336		0.361
R_2 in IV	100.8		101.3	101.0±1.5	0.61	0.65	0.60		0.66
R_1 in V	100.8		101.0	100.9±1.5	0.60	0.66	0.54		0.61
R_3 in VI	102.1		102.1	102.1±1.5	0.62	0.70	0.57		0.65
S_1^2, R_2, S_2^3 in VII	136.4	137.6	134.9	136.3±2	1.17		1.16	1.16	1.31
R_1, R_2, R_3 in VIII	192	194	195	194 +3	2.08	2.50	1.59	1.82	2.08
S_1, S_2 in IX	357	367	360	360 ±8	4.72	5.2	3.26	3.74	4.87
S_1, S_2, S_3, R in X	569	591	577	576 ±15	8.16	12	4.46	6.12	10.1

Tab. II Experimental results for β/Λ found from eq.(3.5) and (3.6)

	β/Λ from eq.(3.5)			$\beta/\Lambda = \gamma$ from eq.(3.6)		
Detector position (cf.fig.1)	(12)	(24)	(3)	(12)	(24)	(3)
Control plate configuration (cf.fig.1)	$[sec^{-1}]$	$[sec^{-1}]$	$[sec^{-1}]$	$[sec^{-1}]$	$[sec^{-1}]$	$[sec^{-1}]$
R_2 : 35.0 cm II	60.0		59.9	61.1		61.1
R_2 : 20.0 cm III	63.0		62.2	62.3		61.7
R_2 in IV	63.0		61.2	62.3		60.1
R_1 in V	65.2		62.7	64.5		62.2
R_3 in VI	65.2		61.8	64.2		62.0
S_1^2, R_2, S_2^3 in VII	65.2	62.4	59.9	61.7	60.6	57.4
R_1, R_2, R_3 in VIII	74.1	68.8	63.4	72.2	66.6	61.0
S_1, S_2 in IX	83.6	77.5	61.4	79.5	78.2	58.3
S_1, S_2, S_3, R in X	106.4	83.1	52.0	91.3	77.8	50.4

The α-values found with the three detector positions are in good agreement, showing that the effects of higher modes have been properly eliminated. From the decay constant $\alpha_c = \beta/\Lambda_c = 62.9 \pm 1.5\ \mathrm{sec}^{-1}$ and the calculated value $\beta = 0.00749$, a generation time $\Lambda_c = 1.19 \cdot 10^{-4}$ sec was found at delayed critical.

The reactivity ρ/β of the various configurations was derived from α on the basis of eq.(3.2) assuming a generation time $\Lambda = \Lambda_c$ independent of ρ. Tab.I compares this value $-\rho/\beta = \alpha/\alpha_c - 1$ with the reactivity $-(\rho/\beta)_s$ found by "rod-drop" and "continuous-run" techniques [10] where the variation of neutron intensity n(t) resulting from a stepwise or continuous insertion of control plates into the critical reactor was measured with a boron chamber and analysed by a digital code which calculates ρ/β as a function of time, i.e. of control plate position. The change in neutron flux observed in these methods is relatively slow, so that $(\rho/\beta)_s$ is expected to be close to the static reactivity. Except for the far subcritical systems ($\rho/\beta \lesssim -2\ \$$) where effects of local control plate shadowing may be present, the $(\rho/\beta)_s$-values were expected to be very reliable. The pulsed source values $-\rho/\beta = \alpha/\alpha_c - 1$ are found to be somewhat lower than $-(\rho/\beta)_s$, even near delayed critical, which might indicate that Λ increases slightly with $-\rho/\beta$ rather than being a constant.

A comparison was also made for $\bar{n}_p/\bar{n}_d$, the ratio of prompt and delayed neutron intensities which would equal $-\rho/\beta$, according to eq.(3.4), if the point reactor model were applicable. As a matter of fact, $\bar{n}_p/\bar{n}_d$ turned out to be strongly dependent on the detector position. That is, for each configuration the ratio $\bar{n}_p/\bar{n}_d$ increases as one proceeds with the detector from the core to the reflector.

This space-dependence of $\bar{n}_p/\bar{n}_d$ is a direct consequence of the different shapes of the static and the dynamic eigenfunctions, i.e. the non-separability of time and space variables, and shows the breakdown of the space-independent model for systems with large reflectors.

A similar behaviour is found for the quantity $\beta/\Lambda = \alpha\ (1 + \bar{n}_p/\bar{n}_d)^{-1}$ which was derived from the experimental values α and $\bar{n}_p/\bar{n}_d$. Tab.II gives a comparison of this quantity with the value $\gamma = \beta/\Lambda$ found by the method of Garelis and Russell, eq.(3.6). Except for minor deviations due to the (positive) contribution of higher modes to $\bar{n}_d$, both methods give the same dependence of β/Λ on the detector position. For $\rho/\beta \to 0$ the β/Λ-values approach $\alpha_c = \beta/\Lambda_c$ as expected (fig.3).

Fig.3

γ vs. $\alpha/\alpha_c - 1$ for different detector positions (cf.fig.1)

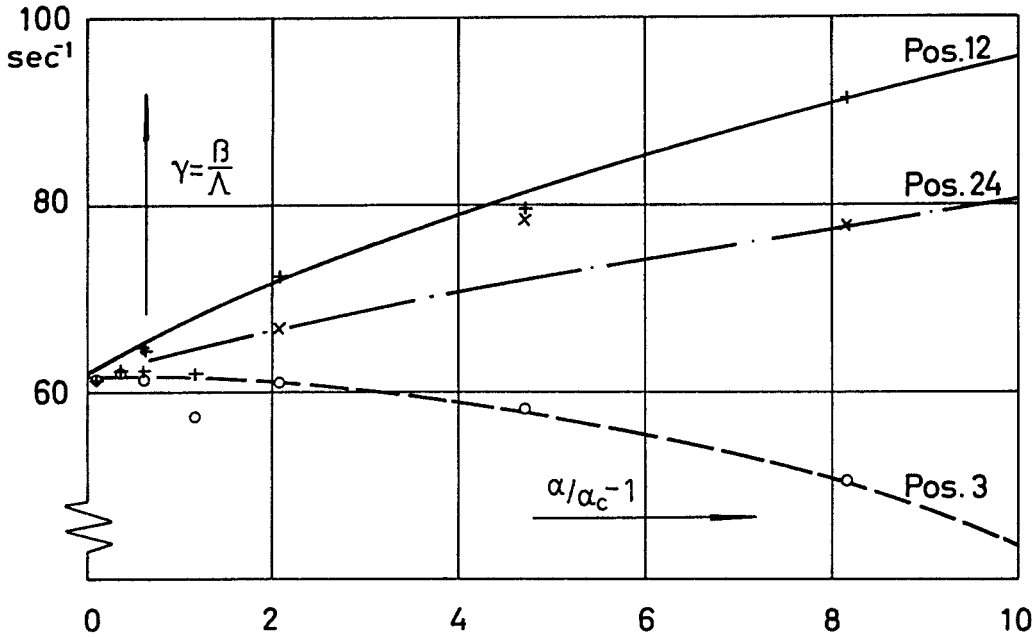

Fig.4

$\alpha/\gamma - 1$ vs. $\alpha/\alpha_c - 1$ for different detector positions (cf.fig.1)

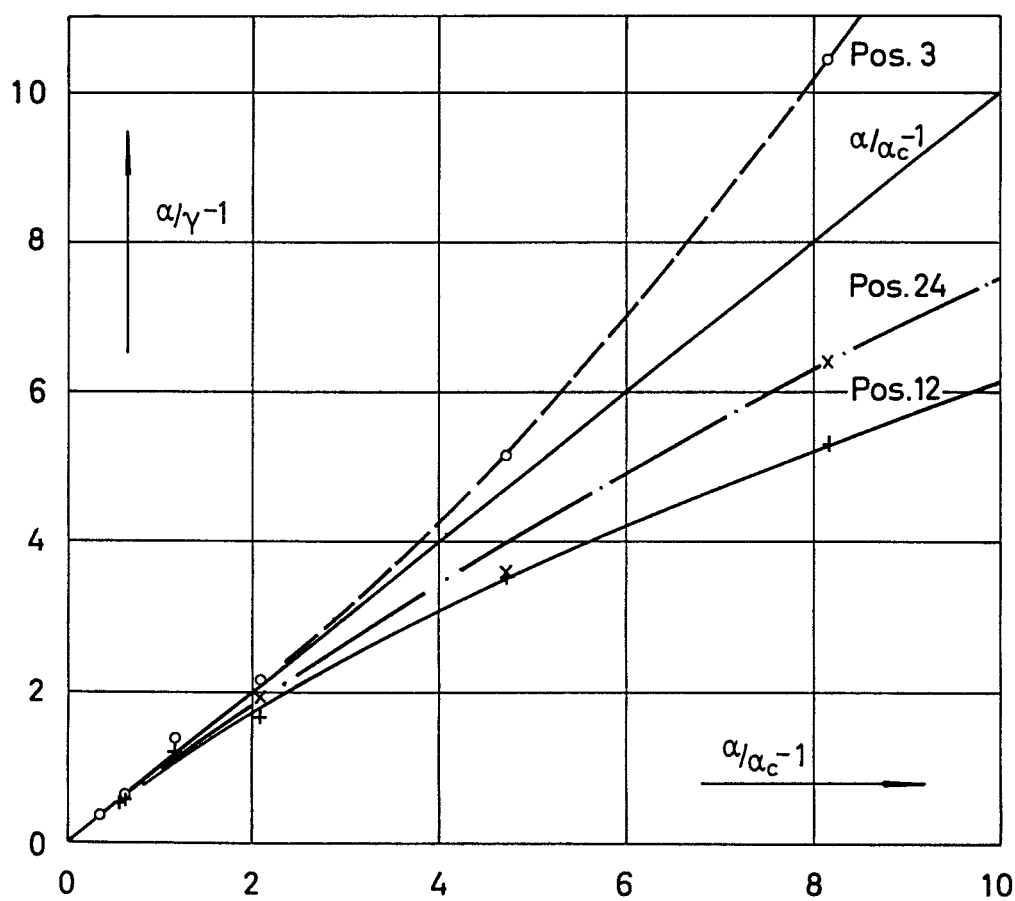

The quantity $\alpha/\gamma - 1$, which would be equal to $-\rho/\beta$ for the point reactor model, is shown in fig.4 as a function of $\alpha/\alpha_c - 1$. Deviations in $\alpha/\gamma-1$ for the various detector positions are increasing with $\alpha/\alpha_c - 1$ up to values as high as 50% at -8 $.

The question arises whether detector and source positions can be found in a reflected system such that the kinetic behaviour of n(t) corresponds to that of a point reactor. This question can only be answered, a priori, by detailed calculations of the static and dynamic eigenfunctions for a particular system. However, it can be shown from reactor theory that eq.(3.4) remains valid for reflected systems for a detector distribution proportional to $\nu\Sigma_f\, n_s^+$, where n_s^+ is the adjoint density of the static problem.

These investigations have shown that the methods based on the point-reactor model to determine ρ/β from the prompt and delayed neutron intensities are of little use for systems like STARK with a small core and a large graphite reflector. On the other hand, no serious problems were encountered in measuring the prompt-neutron decay in such systems by the pulsed neutron technique.

The results found from the pulsed source experiments are compared to those of the other methods in table VI.

4. Statistical experiments

Information on reactor parameters which describe the neutronic behaviour of a zero power reactor can be gained from a detailed analysis of the statistical fluctuations in detector signals. The common basis of all these experiments is the observation of correlated reaction processes due to branching events occurring in neutron chain reacting systems. A number of papers have been published [11 - 22] in which different theorectical models and techniques of analysing the fluctuating signals are discussed. Recently a common theoretical basis has been developed for neutronic noise analysis experiments [23] from which the fundamental equations for the experiments described in the following sections have been derived.

4.1 Rossi-α-experiment

In this experiment correlated detector events due to neutrons from the same chains are directly observed in a stationary reactor.

In the point reactor model approximation the fundamental equation to calculate the correlation function for a Rossi-α-experiment performed with two absorption detectors is given by

$$c(\tau)\,\Delta\tau = \left[A\, e^{-\alpha\tau} + B_2\right]\Delta\tau \qquad (4.1.1)$$

with $\alpha = \frac{1 - k_p}{l} = \frac{1 - k\,(1 - \beta)}{l}$ = prompt neutron decay constant

$$A = W_2 \frac{\chi_2}{2} \frac{k^2}{\alpha\, l^2} \approx W_2 \frac{\chi_2}{2\beta^2} \frac{\alpha_c^2}{\alpha}$$

$B_2 = W_2 F$ = counting rate in detector channel 2 (4.1.2)

$c(\tau)\Delta\tau$ = expected number of counts from detector channel 2 in a time interval $\Delta\tau$ around a time τ following a trigger pulse from detector channel 1 at $\tau = 0$ (crosscorrelation experiment)

F = fission rate in the whole system

k = effective multiplication constant

k_p = prompt neutron multiplication constant

l = prompt neutron lifetime

W_2 = detector efficiency in counts per fission)

$\chi_2 = \frac{\overline{\nu(\nu-1)}_p}{\overline{\nu}^2} \approx 0.8$ (ν = number of neutrons per fission).

Eq.(4.1.1) holds correspondingly also for an autocorrelation experiment in which only one detector channel is used such that the first incoming pulse at $\tau = 0$ and the following pulses, which are to be time analysed come from the same detector. In both versions of the experiment this equation holds exactly only if an experimental setup is used which determines the correlation function by delayed coincidences as in the instrumentation used by Orndoff [11]. In the experiment described here a different electronic system was necessary to apply because it had to be used for measurements of much slower decay constants. The block diagram is shown in fig.5.

The time analyser is a TMC Model CN-110 with Pulsed Neutron Logic Unit 212 which has been slightly modified. The time analysis cycle is started in the crosscorrelation experiment by a trigger pulse from detector channel 1. All pulses from channel 1 arriving during the cycle time are rejected. After a cycle has been started, all pulses from detector channel 2 are sorted into the time channels of the analyser according to their time of arrival. Because of this the system analyses only correlations between single trigger pulses separated by at least one cycle time and signal pulses from detector channel 2

Fig.5

Two Rossi-α runs on STARK with block diagram of apparatus

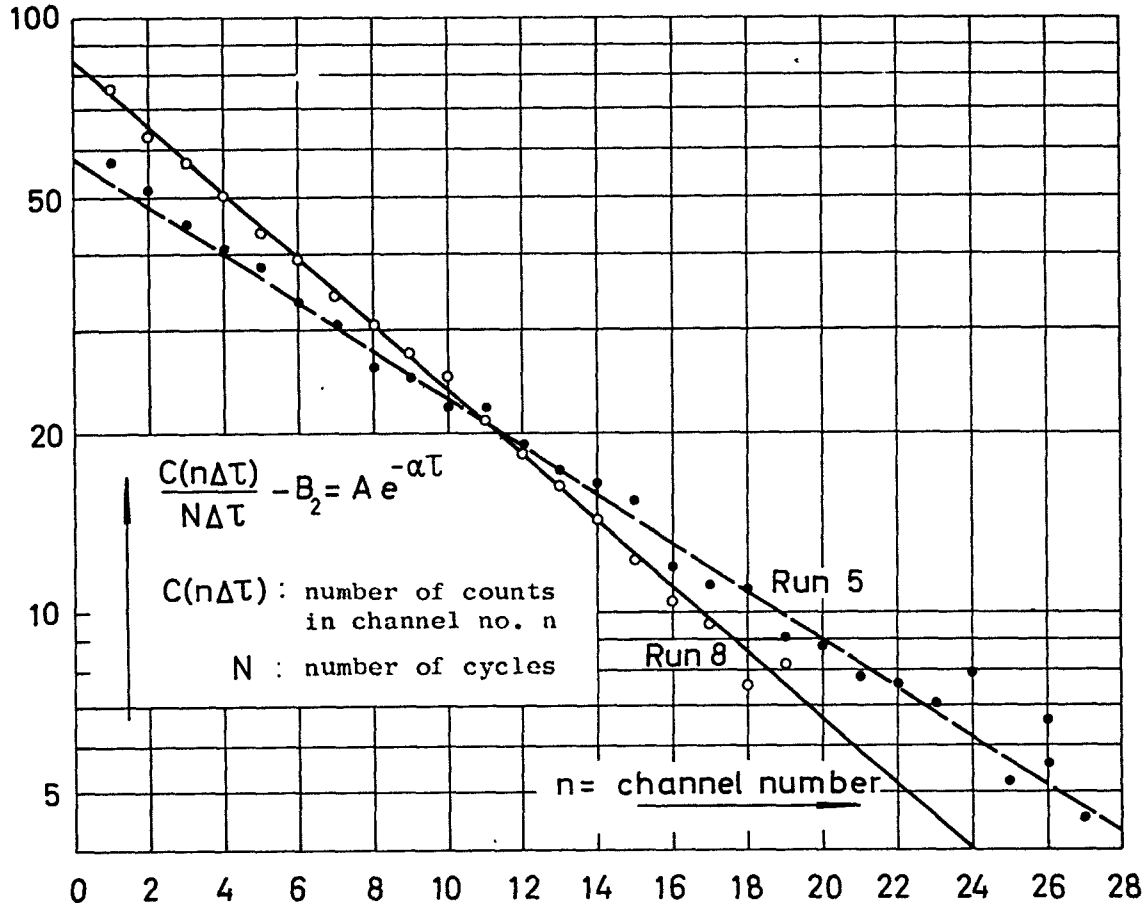

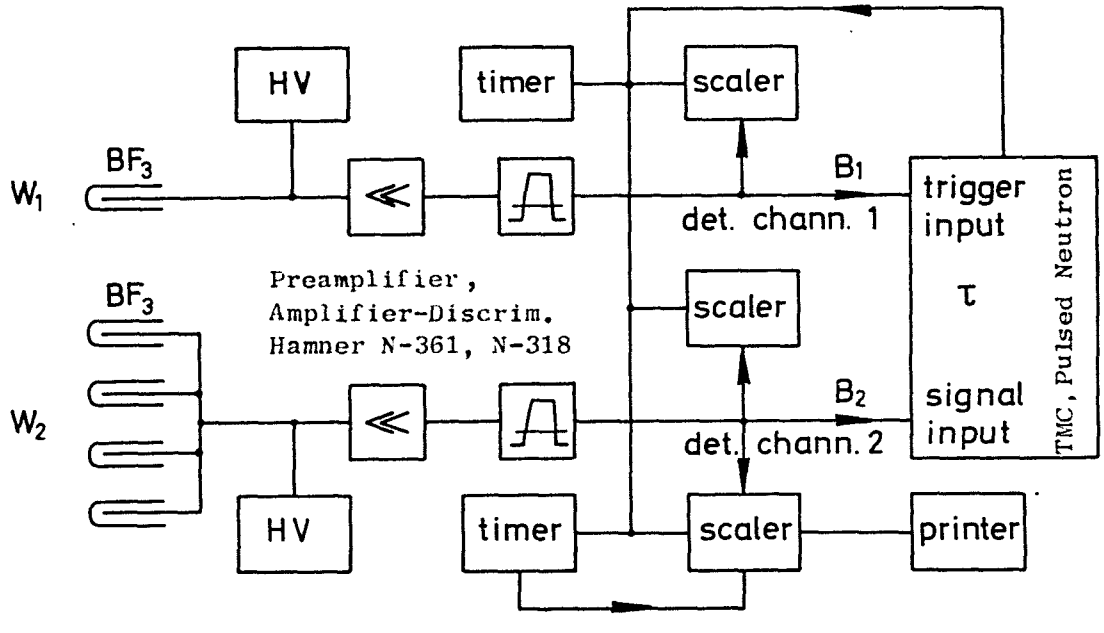

within the cycle time. This leads to a dependency of A and in a less degree also of α on the efficiency W_1 of detector channel 1.

Only the first term $A\ e^{-\alpha\tau}$ of eq.(4.1.1) results from correlated events. The second term B_2 is the contribution due to uncorrelated events. B_2 can be considered to be background in this experiment.

The fission rate F can be calculated from the ratio $\frac{B_2}{A}$,

$$F = \frac{B_2}{A} \cdot \frac{\chi_2}{2\beta^2} \cdot \frac{\alpha_c^2}{\alpha} . \qquad (4.1.3)$$

The efficiency can than be found from (4.1.2). Reactivity values have been calculated using (3.3) with $\alpha_c = 62.9\ sec^{-1}$ from table VI and the neutron source S_o (mainly due to spontaneous fissions in U^{238}) from

$$S_o = F\ (1 - k_p - \beta)\ \bar{\nu} . \qquad (4.1.4)$$

Various experimental runs have been made under the same loading and reactivity conditions specified for the other experiments. The channel width chosen was 640/usec for all runs with the channel numbers ranging from 32 to 128. The results are given in table III. In the first four columns are listed: run number, control plate settings, detector postions (cf.fig.1), and efficiencies estimated from the neutron flux at that position and the reactor power and the boron content in the counting tube. The second part of the table contains measured results for α, A, and B_2 from which the quantities in the last part of the table have been calculated according to eqs.(3.3), (4.1.3), (4.1.2), and (4.1.4).

The signal to background ratio, A/B_2, is inversely proportional to the fission rate and the neutron lifetime in the system. Due to spontaneous fissions in the fairly large amount of U^{238} in the central zone, the fission rate was unfavourably high for the experiments. In addition the neutron lifetime was long. For these reasons it was difficult to perform Rossi-α-experiments near the delayed critical state of this loading of STARK. The results of runs 1 - 3 are therefore of poor quality and have been put into brackets. The fact that only one trigger pulse is accepted during one cycle may result in some preselection of trigger counts, particularly if the trigger channel has a highly efficient detector. From a comparison of run 4 with runs 5 and 6 one finds a noticeable influence of the detector efficiency on the signal to background ratio, so that the derived quantities F and S_o are too large and W_2 is too small in run 4. From run 7 and 8 it may be concluded that not only is the signal to background ratio affected, but also α, which turns out to be too

Tab. III Results of the Rossi-α-experiments

Run No.	Control plate configuration (cf.fig.1)	Detector positions (cf.fig.1)	Detector efficiency (W_1) (W_2)	Measured results α [sec^{-1}] Auto-corr.	Measured results α [sec^{-1}] Cross-corr.	Measured results A [sec^{-1}]	Measured results B_2 [sec^{-1}]	Calculated results ρ/ß [$	Calculated results F [sec^{-1}]	Calculated results W_2 [counts/fiss.]	Calculated results S_o [sec^{-1}]
1	R_2 = 20 cm III	22 21,23,25,27	$1.4 \cdot 10^{-4}$ $7.7 \cdot 10^{-4}$	-	(47)	(37)	2700	-	-	-	-
2	R_2 in IV	22 21,23,25,27	$1.4 \cdot 10^{-4}$ $7.7 \cdot 10^{-4}$	-	(79)	(47)	1500	-	-	-	-
3	R_2 in IV	21 11,12,13,14	$1.9 \cdot 10^{-4}$ $7.9 \cdot 10^{-4}$	-	(92)	(59)	1800	-	-	-	-
4	S_1^2, S_2^3, R_2 in VII	22,24,26,28 21,23,25,27	$5.6 \cdot 10^{-4}$ $7.7 \cdot 10^{-4}$	-	138	32	573	1.19	$(3.6 \cdot 10^{6})$	$(1.6 \cdot 10^{-4})$	$(8.3 \cdot 10^{4})$
5	S_1^2, S_2^3, R_2 in VII	22 21,23,25,27	$1.4 \cdot 10^{-4}$ $7.7 \cdot 10^{-4}$	-	139	58	573	1.20	$(2.0 \cdot 10^{6})$	$(2.9 \cdot 10^{-4})$	$(4.6 \cdot 10^{4})$
6	S_1^2, S_2^3, R_2 in VII	22 21,23,25,27	$1.4 \cdot 10^{-4}$ $7.7 \cdot 10^{-4}$	-	142	56	573	1.25	$(2.0 \cdot 10^{6})$	$(2.8 \cdot 10^{-4})$	$(4.9 \cdot 10^{4})$
7	R_1, R_2, R_3 in VIII	- 21,23,25,27	- $7.7 \cdot 10^{-4}$	(179)	-	(33)	394	(1.84)	$(2.7 \cdot 10^{6})$	$(1.5 \cdot 10^{-4})$	$(9.5 \cdot 10^{4})$
8	R_1, R_2, R_3 in VIII	22 21,23,25,27	$1.4 \cdot 10^{-4}$ $7.7 \cdot 10^{-4}$	-	196	83	394	2.11	$6.8 \cdot 10^{5}$	$5.8 \cdot 10^{-4}$	$2.7 \cdot 10^{4}$

small in run 7 because of the high efficiency used in the run. Using this type of analysing equipment and applying eq.(4.1.1) to the evaluation of the measured data, the restriction has to be considered which limits the efficiency resp. counting rate of the trigger channel to values low enough to eliminate these effects. The results of the Rossi-α-experiment are compared to those of the other methods in table VI.

4.2 Analysis of counting statistics

A new experimental technique has been applied to the measurement of the distribution of probabilities $p_n(T)$ for n detector counts in a specified time interval of length T. Correlated detector counts in chain reacting systems are responsible for the dependence of the variance of the distribution on reactor-physics parameters, i.e. on the multiplication constant k and the prompt neutron decay constant α, as well as on the detector sensitivity, W. In other words the main purpose of this technique is to determine the deviation of the counting statistics from Poisson's law.

An experimental setup was built for the direct measurement of the probabilities $p_n(T)$, where n can range from 0 to 127. This probability distribution analyser [24] is schematically shown in fig.6. The operating principle is as follows: Pulses from one or more detectors are fed into the input A of a fast acting electronic step switch, which proceeds by one step for each incoming pulse. Pulses from a time marker terminating the length T of the time interval are fed into input B. According to the position of the electronic switch, a gate is opened for the time pulse which gives a signal to the scaler connected to this output. If, for instance, 4 counts came in during the interval, output 4 of the switch opens gate 4 so that the pulse from the time marker delivers a signal into scaler 4. Thus 4 counts have been registered during this time interval. The step switch is reset and the probability distribution analyser is opened for a new cycle. After a sufficiently long time the run for one T-value is finished and the probabilities $p_n(T)$ are obtained directly by dividing the number of counts in scaler n, C_n, by the number of counts in the time interval scaler, C_T, giving

$$p_n = \frac{C_n}{C_T} \,. \tag{4.2.1}$$

The performance of the analyser is checked by the monitor scaler, because the relation

$$C_M = \sum_{n=1}^{127} n \cdot C_n \tag{4.2.2}$$

must be satisfied for the number of counts in the monitor scaler, C_M. An additional check is given by

$$C_T = \sum_{n=0}^{127} C_n \quad . \tag{4.2.3}$$

From this distribution of probabilities $p_n(T)$ the following mean values may be computed:

$$\bar{n}\,(T) = \sum_{n=1}^{\infty} p_n(T) \cdot n \tag{4.2.4}$$

$$\overline{n^2}(T) = \sum_{n=1}^{\infty} p_n(T) \cdot n^2 \tag{4.2.5}$$

$$\overline{n(n-1)}(T) - \bar{n}^2(T) = \sum_{n=2}^{\infty} p_n(T) \cdot n(n-1) - \left[\sum_{n=1}^{\infty} p_n(T) \cdot n \right]^2 \quad . \tag{4.2.6}$$

As has been shown earlier [14,15,23] in the point reactor model approximation, the equation to calculate the reactor physics parameters is given by

$$\frac{\overline{n^2}(T) - \bar{n}^2(T) - \bar{n}(T)}{T^2} = \frac{\bar{n}(T)}{T} \cdot \frac{W \cdot \chi_2 \cdot k^2}{\alpha l^2} \cdot \frac{e^{-\alpha T} - 1 + \alpha T}{(\alpha T)^2} \quad . \tag{4.2.7a}$$

with the symbols defined as in section 4.1.

The numerator on the left hand side contains the difference between the measured variance $(\overline{n^2} - \bar{n}^2)$ and the variance of a POISSON distribution, which is equal to $\bar{n}$. A rearrangement of this equation leads to an equivalent formulation

$$Y(T) = \frac{\overline{n(n-1)}(T) - \bar{n}^2(T)}{\bar{n}(T)} = W \cdot \chi_2 \cdot \frac{k^2}{(1-k_p)^2} \left[1 - \frac{1 - e^{-\alpha T}}{\alpha T} \right] \tag{4.2.7b}$$

which has been used for the evaluation of the experimental results.

This expression consists of two distinct terms. The second one within the brackets approaches unity for $T \to \infty$. From the first one, which near the delayed critical state is also given by

$$Y_\infty = W \cdot \chi_2 \cdot \frac{k^2}{(1-k_p)^2} = W \cdot \chi_2 \cdot \frac{1}{\beta^2} \cdot \left[\frac{\alpha_c}{\alpha} \right]^2$$

the efficiency W can be calculated if α_c, α, and β are known. The absolute fission rate follows from

$$F = \frac{C}{W}$$

where C is the counting rate in the experiment. The neutron source strength S_o can directly be determined using (4.1.4).

Tab. IV Results of the analysis of counting statistics

Run No.	Control plate configuration (cf.fig.1)	Detector position (cf.fig.1)	$\alpha\,[\mathrm{sec}^{-1}]$	Y_∞	$\frac{\rho}{\beta}\,[\$]$	W [counts/fiss.]	C $[\mathrm{sec}^{-1}]$	F $\left[\frac{\text{fissions}}{\text{sec}}\right]$	$S_o\left[\frac{\text{neutrons}}{\text{sec}}\right]$
1	R_2 35 cm II	24	69.5	0.234	-0.10	$2.02\cdot10^{-5}$	245	$1.21\cdot10^{7}$	$2.27\cdot10^{4}$
2	R_2 20 cm III	22	82.3	0.818	-0.31	$9.8\cdot10^{-5}$	370	$3.78\cdot10^{6}$	$2.19\cdot10^{4}$
3	R_2 in IV	22	111.5	1.03	-0.77	$2.28\cdot10^{-4}$	391	$1.72\cdot10^{6}$	$2.48\cdot10^{4}$
4	S_1^2 S_2^3 R_2 in VII	22	161	0.563	-1.56	$2.58\cdot10^{-4}$	183	$7.09\cdot10^{5}$	$2.06\cdot10^{4}$
5	S_1^2 S_2^3 R_2 in VII	21,23,25,27	138	1.73	-1.19	$5.84\cdot10^{-4}$	575	$9.85\cdot10^{5}$	$2.20\cdot10^{4}$
6	R_1 R_2 R_3 in VIII	21,23,25,27	216	0.929	-2.43	$7.68\cdot10^{-4}$	395	$5.14\cdot10^{5}$	$2.34\cdot10^{4}$
7	R_1 R_2 R_3 in VIII	21,23,25,27	212	1.027	-2.37	$8.18\cdot10^{-4}$	395	$4.83\cdot10^{5}$	$2.14\cdot10^{4}$

Remarks: Detectors listed in one row were connected in parallel.
To calculate the reactivity, $\alpha_c = 62.9\ \mathrm{sec}^{-1}$ has been taken from table VI.
$\beta = 7.5\cdot10^{-3}$ (calculated); $\bar{\nu} = 2.5$.

Fig.7

Y(T)-curves from the analysis of counting statistics

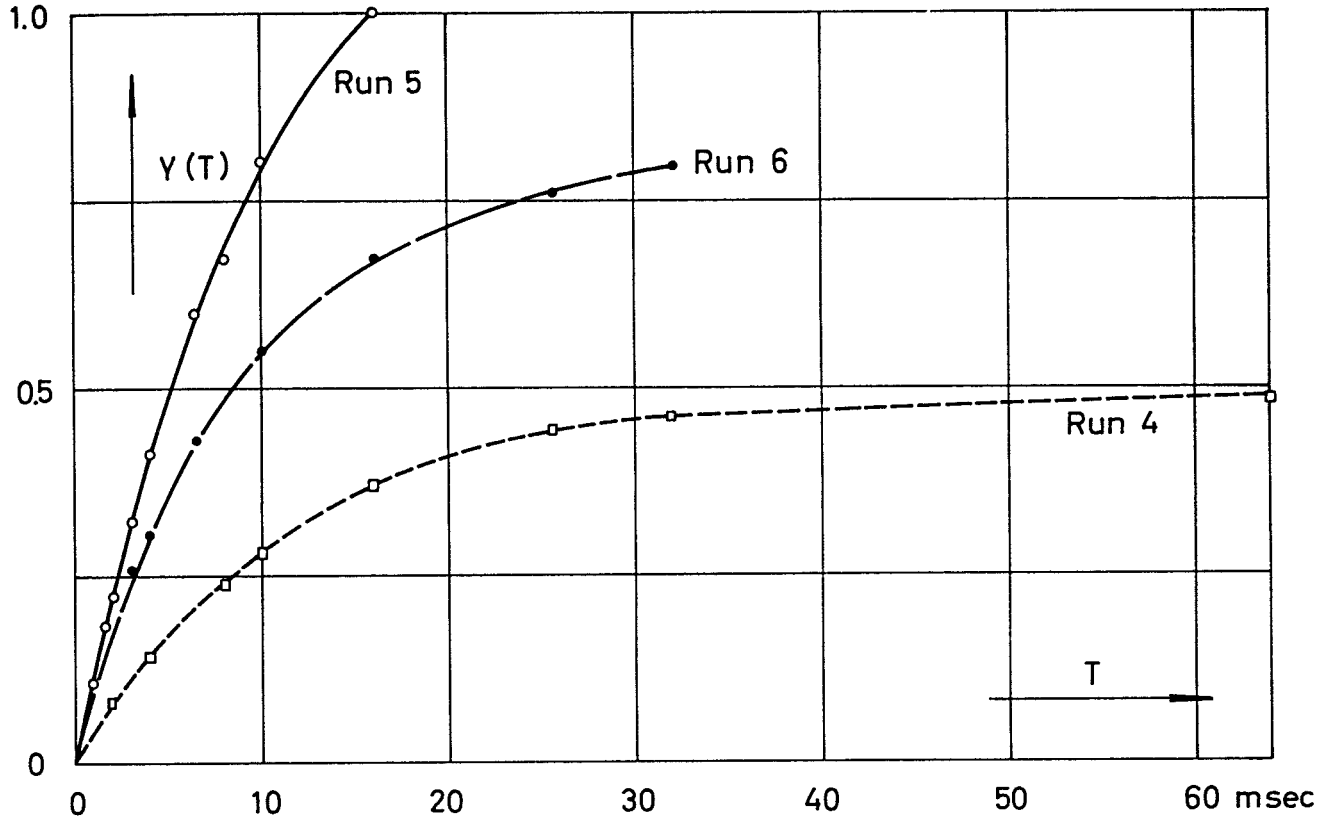

Fig.6

Schematic diagram of the probability distribution analyser

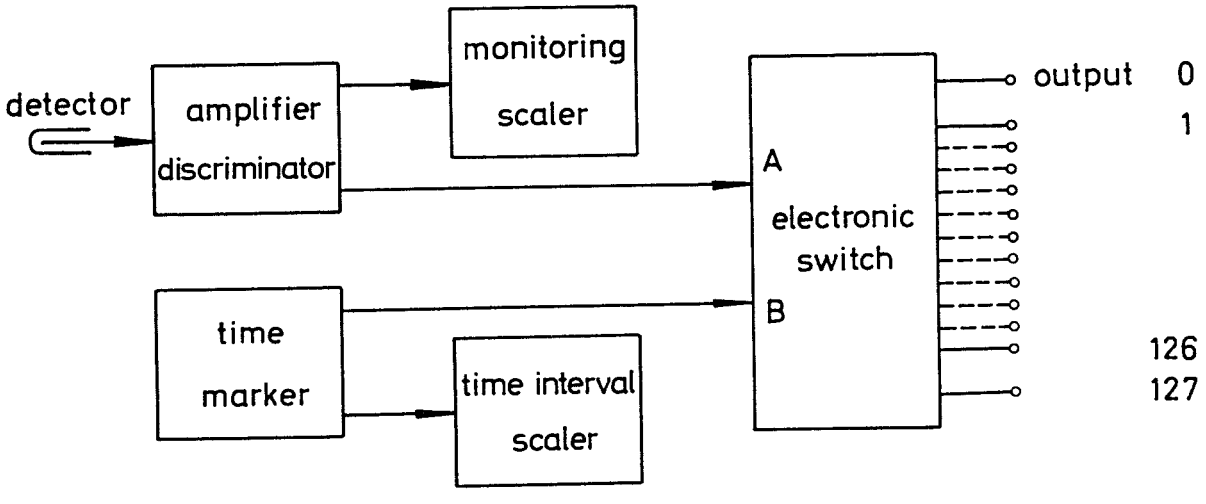

The experiments were performed under the same loading and reactivity conditions as with the other methods described in this paper. The various experimental runs are listed in table IV. For each run different time intervals were chosen so that several probability distributions were measured, from which Y(T) could be calculated. To assure good statistical accuracy at least 10^5 counts have been analysed for each distribution. The Y(T)-curves for three runs listed in table IV are shown in fig.7. The quantities α and Y_{oo} were computed from these curves by a least squares fit. These results, as well as the calculated efficiency W, fission rate F and source strength S_o, are given in the table.

Measurements could not be made at delayed critical because of small reactivity and power changes with time due to the temperature coefficient in the heated thermal core section. The results obtained for the fission rates are in good agreement with the foil activation measurements which were used to calibrate the reactor instrumentation. The values found for the source strength S_o, which should be a constant for all runs, agree within $\pm$10%. A comparison with the results of the other techniques is given in table VI.

4.3 Frequency analysis of reactor noise

In this experiment the observation of correlated events is performed in the frequency domain by analysing the fluctuations of ion-chamber currents. This can be done by a single-detector-experiment (autocorrelation) or by the more flexible two-detector-experiment (crosscorrelation). The block diagram is shown in fig.8. The fundamental equations, derived from the common theoretical basis [23] , are given in the point reactor and high frequency approximation (no delayed neutrons) by

$$\text{APSD} = \frac{\overline{r^2}(\omega,\Delta\omega)}{\Gamma(\omega,\Delta\omega)} = W\cdot F\cdot\bar{q}^2\left[R + \frac{W\cdot\chi_2 k^2}{l^2(\alpha^2+\omega^2)}\right] \qquad (4.3.1)$$

for the autocorrelation-experiment and by

$$\text{CPSD} = \frac{\overline{r_1\cdot r_2}(\omega,\Delta\omega)}{\Gamma(\omega,\Delta\omega)} = \bar{q}_1\cdot\bar{q}_2\cdot F\cdot\frac{W_1\cdot W_2\cdot\chi_2 k^2}{l^2(\alpha^2+\omega^2)} \qquad (4.3.2)$$

for the crosscorrelation-experiment. The symbols W, F, χ_2, k, l and α were already defined in section 4.1. The others are

APSD = auto-power-spectral-density

CPSD = cross-power-spectral-density

r_n = chamber current (chamber n)

$\Gamma(\omega,\Delta\omega)$ = band width of filters = $\mathrm{Re} \int_0^\infty \frac{d\omega'}{\pi} B_1(\omega') B_2(-\omega')$

$B_n(\omega)$ = frequency characteristic of filter n

ω = $2\pi f$ = angular frequency

$\Delta\omega$ = frequency interval

$\bar{q}_n$ = average charge per detected neutron

$R = \frac{\overline{q^2}}{\bar{q}^2}$

From a comparison of eqs.(4.3.1) and (4.3.2) it can be seen that the contribution due to uncorrelated noise (first term on the right hand side of eq.(4.3.1)) is not present in the cross-correlation experiment. This is a specific feature of the two-detector-experiment and is particularly important in all cases where the uncorrelated contribution is relatively large. The expression for the fission rate F is particularly simple if the experiment is performed in the low frequency range ($\omega \ll \alpha$). In this case

$$F = \frac{\chi_2}{\beta^2}\left[\frac{\alpha_c}{\alpha}\right]^2 \frac{\bar{i}_1 \cdot \bar{i}_2 \cdot \Gamma(\omega,\Delta\omega)}{\overline{r_1 \cdot r_2}\,(\omega,\Delta\omega)} \qquad (4.3.3)$$

where

$$\bar{i}_n = \bar{q}_n \cdot W_n \cdot F \qquad n = 1, 2 \qquad (4.3.4)$$

is the mean current of the ion chamber n. If F has been calculated, $\bar{q}_n \cdot W_n$ is easily found from eq.(4.3.4).

The block diagram of the experimental setup used for the cross- and autocorrelation measurements is shown in fig.8. The current fluctuations of the ion chambers (Type RC 6) are amplified in electrometer amplifiers (Keithley 603) and fed into bandpassfilters (Krohn Hite 330 M). The filter output signals are multiplied (in a two-detector-experiment) or squared (in a single-detector-experiment) and integrated for a specified time T with analogue computing equipment (Pace TR 10) to give the mean value. The integrated voltage was converted into a digital form by use of an analog-to-digital converter (Dymec 2210) and a normal pulse scaler.

Several experimental runs have been made under the specified loading condition (cf. section 2) in the autocorrelation and crosscorrelation version of the method. The results of characteristic examples are listed in table V. The positions of the two ion chambers used, are indicated in fig.1.

Tab. V Results of frequency analysis measurements

Run No.	Control plate configuration (cf.fig.1)	Method	Detector position (cf.fig.1)	α [sec^{-1}]	$W_1 \bar{q}_1$ [10^{-18} amp sec/fiss.]	$W_2 \bar{q}_2$ [10^{-18} amp sec/fiss.]	Reactor power instrum. (foil act.)	Reactor power frequency analysis
1	del. critical	auto	K	65	2.0	-	10 W	12 W
2	del. critical	cross	K, W	61.7	2.1	1.2	10 W	11.7 W
3	del. critical	cross	K, W	65	2.4	1.3	0.1 W	0.11 W
4	R_2 : 35.0 cm	cross	K, W	67	-	-	400 μ W	400 μ W
5	R_2 : 20.0 cm	cross	K, W	85	-	-	100 μ W	120 μ W

Fig.9

Power Spectral Density
for single-detector (upper curve)
and two-detector-experiment (lower curve)

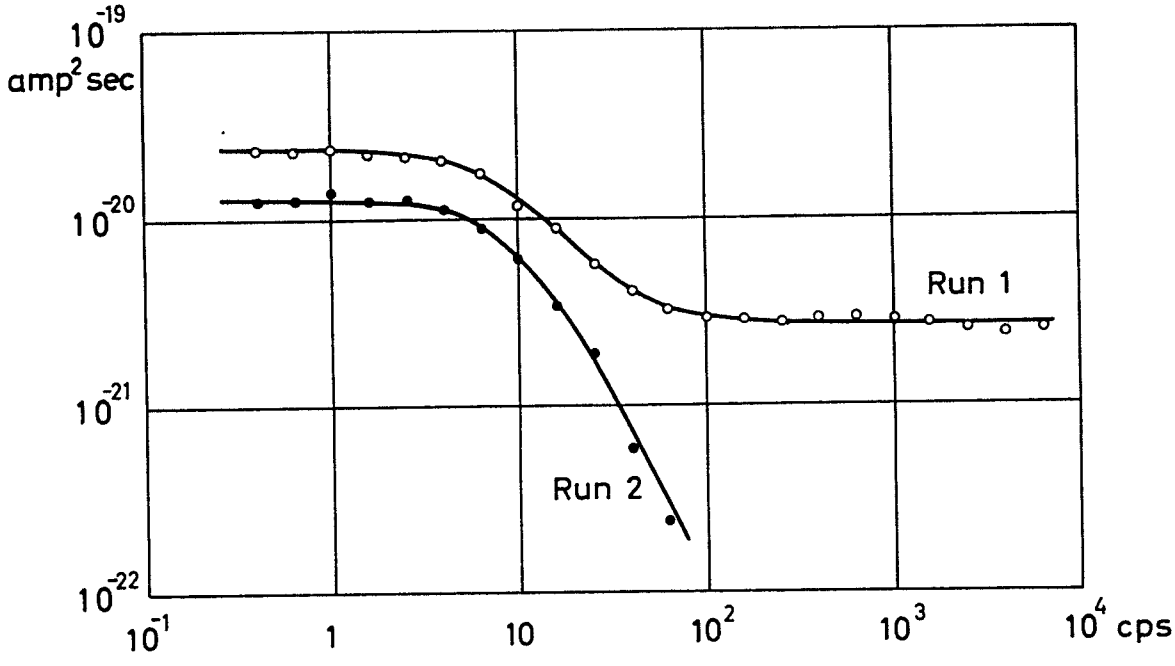

Fig.6

Block diagram for measurement of
Cross Power Spectral Density

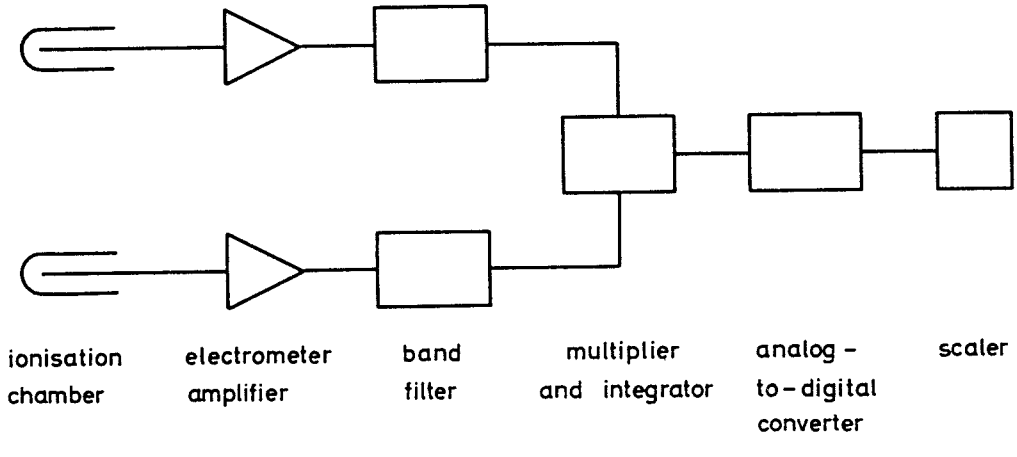

The prompt neutron decay constant α was determined by a least squares fit from the measured power spectral density versus frequency curves. Two examples, one for an autocorrelation (upper curve) and one for a crosscorrelation measurement (lower curve), are shown in fig.9. The advantage of the two-detector-experiment is clearly seen from the curves. The absolute fission rate F was calculated using eq.(4.3.3). The comparison to the results found by foil activation, with which the reactor instrumentation was calibrated, shows that somewhat larger values were obtained by the frequency analysis technique. The values for $W_1\bar{q}_1$ and $W_2\bar{q}_2$ are also listed for comparison. Measurements more subcritical than indicated in the table could not be performed because of interfering effects in the electronic system. The results obtained by this technique are compared with the other results in table VI.

5. Comparison of results and conclusions

The comparable results of the different methods are listed in table VI. The α-values have been averaged if more than one run has been made under the same conditions or if no differences were found for various detector positions. The individual numbers are found in tables I - V. For the calculation of reactivity from α and α_c the pulsed neutron results have been taken for simplicity to compare reactivity values with the rod drop- or continuous run-data.

The comparison of measured prompt neutron decay constants in table VI shows good agreement between the four methods in general. From the delayed critical state (I) to the control plate configuration III the results agree well within the error limits of about $\pm$3%. For configuration IV and particularly for VII with detector postion 22 the discrepancy between the pulsed source and counting statistics data amounts up to 18%. This might be due to the inclusion of higher harmonics contributions in the data of the counting statistics analysis if only one detector position (22) is used in this system. This explanation is supported by the fact that the agreement with the pulsed source data is within 2% if several detectors - distributed properly in the system - were used. The reason for the appearance of such discrepancies lies in the fact that in the pulsed neutron source technique contributions of higher harmonics are eliminated by excluding the first part of the n(t)-curve when α is determined from the exponential slope. In the analysis of counting statistics, on the other hand, all higher harmonics effects are included in the Y(T)-curve from which the prompt neutron decay constant is derived.

Tab. VI Comparison of results

Control plate configuration (cf. fig.1)	Pulsed source		Rossi-α		Count. statistics		Frequency analysis		Pulsed source	Static Meas.
	Detector position	$\alpha\,[\mathrm{sec}^{-1}]$	Detector position	$\alpha\,[\mathrm{sec}^{-1}]$	Detector position	$\alpha\,[\mathrm{sec}^{-1}]$	Detector position	$\alpha\,[\mathrm{sec}^{-1}]$	$-\frac{\rho}{\beta}=\frac{\alpha}{\alpha_c}-1\,[\$]$	$-(\frac{\rho}{\beta})_s\,[\$]$
Delayed critical I	12, 3	62.9	-	-	-	-	K,W(cross) K (auto)	63.4	-	-
R_2: 35.0 cm II	12, 3	69.2	-	-	24	69.5	K,W(cross)	67	0.100	0.085
R_2: 20.0 cm III	12, 3	85.3	-	-	22	82.3	K,W(cross)	85	0.356	0.332
R_2 in IV	12, 3	101.0	-	-	22	111.5	-	-	0.61	0.65
S_1^2, R_2, S_2^3 in VII	12,24,3	136.3	21-28	138	21,23,25,27	138	-	-	1.17	-
S_1^2, R_2, S_2^3 in VII	-	-	21,22,23,25,27	140.5	22	161	-	-	-	-
R_1, R_2, R_3 in VIII	12,24,3	194	21,22,23,25,27	196	21,23,25,27	214	-	-	2.08	2.50
S_1, S_2 in IX	12,24,3	360	-	-	-	-	-	-	4.72	5.2
S_1, S_2, S_3, R in X	12,24,3	576	-	-	-	-	-	-	8.16	12

From the comparison of the results the prompt neutron decay constant seems to be the least affected by detector position in a multi region reactor system with special geometry like STARK. The comparison with the other quantities derived from the pulsed source technique showed a much stronger dependency in this regard, indicating, as expected that space independent models cannot be applied to systems with large reflectors.

A few remarks may be added to the applicability of the different techniques to determine the prompt neutron decay constant from the results obtained with loading 1 of STARK. From delayed critical to about -0.5 $ sub delayed critical, in the pulsed neutron technique exact corrections for the time dependent background due to delayed neutrons and eventually a spontaneous fission source are important for the evaluation of the data. In this reactivity range the Rossi-α-technique is difficult to apply in thermal systems with strong sources because of the small signal-to-background ratio caused by the long lifetime and the relatively large fission rate. No difficulties exist for the analysis of counting statistics near and at delayed critical if the power is sufficiently stable. Such is not the case in STARK at delayed critical and at low power level (necessary for moderate counting rates) because of temperature effects. Very reliable results in this range can be obtained from the frequency analysis of noise without any corrections. Difficulties arose, however, below -0.5 $ with this technique which are not of fundamental nature and could be overcome by use of other equipment. All other methods worked well below -0.5 $ to about -3 $. In the more subcritical states the effects of higher harmonics have to be taken into consideration, particularly in the case of the pulsed source n(t)-curves.

Acknowledgement

The authors appreciate the help and cooperation given by Dr.W.Eyrich in constructing and operating the pulsed neutron source. They also wish to thank Mr. H.Borgwaldt for stimulating discussions and help in writing auxiliary computer codes. The authors also acknowledge the support given by the operating staff of the STARK-reactor, in particular Mr. C.Brückner.

References

[1] MEISTER, H., BECKURTS, K.H., HÄFELE, W., KÖHLER, W.H., and OTT, K., KFK-Report No. 217 (1964).

[2] SIMMONS, B.E. and KING, J.S., Nucl. Science and Eng. 3 (1958) 595-608.

[3] SJÖSTRAND, N.G., Arkiv for Fysik 11 (1956) 233-246.

[4] GOZANI, T., Nukleonik 4 (1962) 348/349.

[5] GARELIS, E. and RUSSELL, J.L. Jr., Nucl. Science and Eng. 16 (1963) 263-270.

[6] GARELIS, E., Nucl. Science and Eng. 18 (1964) 242-245.

[7] GARELIS, E., Nucl. Science and Eng. 19 (1964) 131-133.

[8] LEWINS, J., Nucl. Science and Eng. 7 (1960) 122-126.

[9] EYRICH, W. and SCHMIDT, A., SM 62/4.

[10] CARPENTER, S.G., AI-8549, V (1963).

[11] ORNDOFF, J.D., Nucl. Sci. and Eng. 2 (1957) 450.

[12] BRUNSON, G.S., CURRAN, R. et al., Nucleonics 15, No. 11 (1957) 132.

[13] BORGWALDT, H., SANITZ, D., Nukleonik 5 (1963) 239.

[14] BENGSTON, J., 2nd Geneva Conf. 12 (1958) 63.

[15] ALBRECHT, R.W., Nucl. Sci. and Eng. 14 (1962) 153.

[16] ZOLOTUKHIN, V.G. and MOGILNER, A.I., Atomnaya Energiya 15 (1963) 11.

[17] MOORE, M.N., Nucl. Sci. and Eng. 6 (1959) 448.

[18] COHN, C.E., Nucl. Sci. and Eng. 7 (1960) 472.

[19] BENNETT, E.F., Nucl. Sci. and Eng. 8 (1960) 53.

[20] GRIFFIN, C.W., RANDALL, R.L., Nucl. Sci. and Eng. 15 (1963) 131.

[21] SCHRÖDER, R., Nukleonik 4 (1962) 227.

[22] SCHULTZ, M.A., Symp. on Noise Analysis in Nucl. Systems, TID 7679 (1964) 135.

[23] BORGWALDT, H., STEGEMANN, D., Nukleonik in press.

[24] STEGEMANN, D., To be published.

List of figures and tables